Proceedings of ASME Turbo Expo 2011
GT2011
June 6-10, 2011, Vancouver, British Columbia, Canada

GT2011-45168

EXPERIMENTAL AND ANALYTICAL STUDY ON THE OPERATION CHARACTERISTICS OF THE AHAT SYSTEM

Hidefumi Araki, Tomomi Koganezawa, Chihiro Myouren, Shinichi Higuchi
Hitachi, Ltd., Energy and Environmental Systems Laboratory
Hitachi, Ibaraki, Japan

Toru Takahashi
Central Research Institute of Electric Power Industry
Yokosuka, Kanagawa, Japan

Takashi Eta
Sumitomo Precision Products Co., Ltd.
Amagasaki, Hyougo, Japan

ABSTRACT

Operational flexibility, such as faster start-up time or faster load change rate, and higher thermal efficiency, have become more and more important for recent thermal power systems. The AHAT (advanced humid air turbine) system has been studied to improve operational flexibility and thermal efficiency of the gas turbine power generation system. AHAT is an original system which substitutes the WAC (water atomization cooling) system for the intercooler system of the HAT cycle. A 3MW pilot plant, which is composed of a gas turbine, a humidification tower, a recuperator and a water recovery system, was built in 2006 to verify feasibility of the AHAT system.

In this paper, ambient temperature effects, part-load characteristics and start-up characteristics of the AHAT system were studied both experimentally and analytically. Also, change in heat transfer characteristics of the recuperator of the 3MW pilot plant was evaluated from November 2006 to February 2010. Ambient temperature effects and part-load characteristics of the 3MW pilot plant were compared with heat and material balance calculation results. Then, these characteristics of the AHAT and the CC (combined cycle) systems were compared assuming they were composed of mid-sized industrial gas turbines.

The measured cold start-up time of the 3MW AHAT pilot plant was about 60min, which was dominated by the heat capacities of the plant equipment. The gas turbine was operated a total of 34 times during this period (November 2006 to February 2010), but no interannual changes were observed in pressure drops, temperature effectiveness, and the overall heat transfer coefficient of the recuperator.

[*Keywords:* HAT cycle, gas turbine, humidification, part-load characteristics, start-up time, recuperator]

INTRODUCTION

In May 2010, the Japanese Diet approved the legislation, "Basic Act on Global Warming Countermeasures," which aims at a 25% reduction of greenhouse gas emissions by 2020 compared to the 1990 level [1]. The "Basic Policy for Energy Demand and Supply" which was instigated by the Ministry of Economy, Trade and Industry of Japan in June 2010 [2], has defined thermal power generation as an essential technology from the viewpoint of energy security and economy, especially when stabilization of the power grid is needed due to a full-scale adoption of electricity generated from renewable energy sources.

We have been studying the AHAT system [3-15] which can fulfill the requirements for the latest thermal power generation systems, i.e., providing higher thermal efficiency and operational flexibility. Figure 1 (from [13]) shows calculated thermal efficiency of the AHAT system, along with that of existing gas turbine systems.

The AHAT system is an original gas turbine power generation system which substitutes the WAC system for the intercooler system of the HAT [16] cycle. An advantage of the AHAT system, compared with the HAT cycle, is that it can utilize a heavy duty, single-shaft gas turbine which is commonly used for power generation. The AHAT system can achieve the same thermal efficiency as the HAT cycle, at lower pressure ratio than the HAT cycle [4].

The HAT cycle was first presented at the 1983 International Gas Turbine Congress held in Tokyo [17]. Then in 1991, a comparison of the HAT cycle and the NGCC (natural gas combined cycle) was carried out by EPRI [18]. In 1993, a national project in Sweden was begun, and the world's first humid air gas turbine (EvGT) pilot plant, which had a rated power of 600kW, was built [19,20]. During operations of the

EvGT pilot plant, part-load characteristics [19], start-up method [20], characteristics of the humidification tower [21], and water circuit chemistry [22] were studied. However, regarding the part-load characteristics, comparisons between the measured and calculated results were not carried out.

In 2006, to verify the feasibility of the AHAT system, we built a 3MW AHAT pilot plant [8,9,11-15]. We studied operation characteristics of the AHAT [10], and found that ambient temperature characteristics and part-load characteristics of the AHAT were better than those of the CC. However, comparisons between the measurement and the calculation results were not made.

Lorenz [23] calculated the part-load characteristics of the mid-sized EvGT system composed of a commercial 20MW class aero-derivative gas turbine. In this thesis, a comparison between calculated results of the simple cycle gas turbine and measured results of the 600kW pilot plant in simple cycle operation mode was made, but no comparison was made for the EvGT cycle.

Wang et al.[24] compared ambient temperature effects and characteristics of the HAT cycle and those of some other gas turbine cycles such as the simple cycle, the recuperated cycle, the RWI (recuperated water injected) cycle and STIG (steam injection gas turbine). Their calculation model included a stage-by-stage cooled turbine model, a one-dimensional saturator model, and a heat exchanger model based on the effectiveness-NTU methodology. However, comparisons between the measured and calculated results of the whole HAT cycle plant were not made.

One of the distinctive features expected from the AHAT is the faster start-up time compared with an ordinary CC system. Start-up time of the HAT cycle was studied experimentally by some EvGT researchers [20]. They compared two start-up methods. In the first method, the water circuit and the gas turbine were operated separately up to about 15% load where the humidification tower started operation. In the second method, the gas turbine was started with the humidification process fully integrated from the beginning. The estimated start-up times from a cold engine to full load were less than 45min and 5min, respectively for each start-up method. However, it is very difficult for us to estimate the start-up time of the AHAT system, if we do not use a lightweight primary surface type recuperator as used in the EvGT pilot plant.

One of the most important apparatuses in the AHAT system is the recuperator which needs to operate under the high humidity condition. Regarding the recuperator of the SMGT (super marine gas turbine) which burns heavy oil, changes in heat transfer characteristics such as temperature effectiveness and exhaust gas pressure loss have been found [25]. These changes were due to soot deposition on the heat transfer surface. However, for the recuperator of the humid air gas turbine, changes in heat transfer characteristics during the operation have not been reported yet.

In the present study, our first purpose was to study the following operation characteristics of the 3MW AHAT pilot plant: (1) ambient temperature effects; (2) part-load characteristics; (3) start-up characteristics; and (4) change in heat transfer characteristics of the recuperator. Our second purpose was to compare the ambient temperature effects and part-load characteristics of the AHAT with the CC assuming they were composed of mid-sized industrial gas turbines.

3MW AHAT PILOT PLANT

Figure 2 shows a schematic of the AHAT system. There is no intercooler; instead power reduction of the compressor is achieved by the WAC system. The heat is recovered by the air cooler installed in the compressor exit and by the economizer installed downstream from the recuperator. Then, circulated water is heated and fed to the humidification tower and compressed air is humidified to saturation. By adding humidity of about 15-20 weight %, the flow rate and the specific heat of

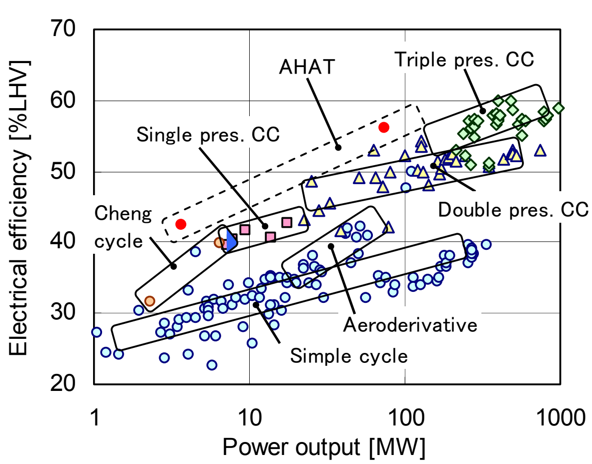

Figure 1 Calculated thermal efficiency of AHAT and other gas turbine systems.

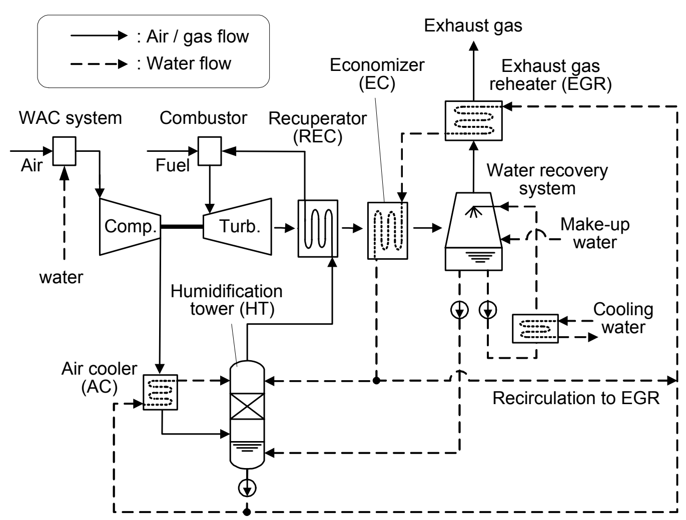

Figure 2 Schematic of the AHAT system.

the working fluid can be increased without increasing the compressor power. As a result, shaft power and thermal efficiency can be greatly improved compared with the recuperated cycle without humidification. The water vapor contained in the exhaust gas is recovered at the water recovery system and it is fed to the circulating water again.

The 3MW pilot plant was built in Hitachinaka City, Japan, to verify feasibility of the AHAT system in 2006. Table 1 shows the design targets of the pilot plant. The gas turbine includes a two-stage centrifugal compressor, a two-stage axial flow turbine, and a cluster nozzle burner. Because the capacity of the turbine must be larger than that of the compressor, unlike usual gas turbines, the gas turbine was specially designed for the AHAT system. Further, the cluster nozzle burner was designed to deal with issues of both flame stability and NOx reduction under high humidity. The plant also has an air cooler, a humidification tower, a recuperator, an economizer and a water recovery system. A photo of the pilot plant is shown in Figure 3.

Table 1 Design targets of pilot plant.

Item	Unit	Value
Rated power output	kW	3,680
Electrical efficiency	%LHV	42.46
Gas turbine speed	min^{-1}	17,800
Inlet air flow	kg/s	10.3
Pressure ratio	-	8.1:1
Turbine entry temperature	ºC	1,180
Turbine exhaust temperature	ºC	669
WAC flow ratio (inlet air flow basis)	%	1.5
NOx emissions (@15%O_2)	ppm	<10

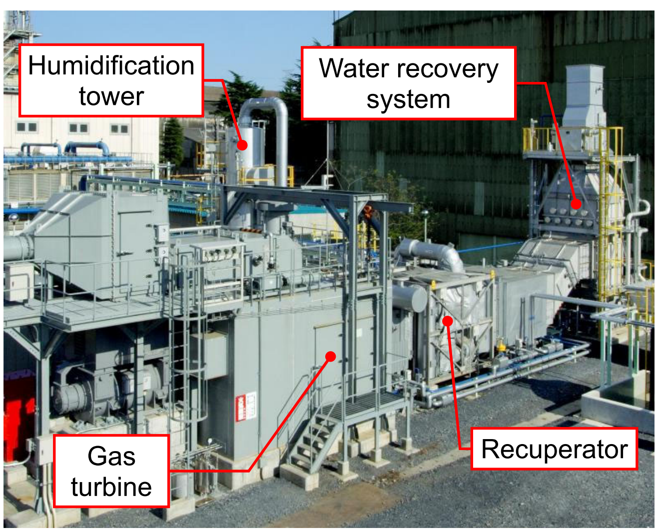

Figure 3 Photo of the 3MW AHAT pilot plant.

AMBIENT TEMPERATURE EFFECTS

Measurements of 3MW Pilot Plant

The 3MW plant was operated from October 2006 to February 2010 under various ambient temperature conditions from 4ºC to 36ºC. Figure 4 shows the ambient temperature effects seen in the 3MW pilot plant. Solid lines show the predicted power output and electrical efficiency. Symbols show corrected power output and electrical efficiency derived from measurements. Because the gas turbine was operated at constant power output, not at constant turbine entry temperature, power output and electrical efficiency were corrected by the heat and material balance calculation, assuming turbine entry temperature was the base condition as shown in the Appendix.

The measured electrical efficiency at 15ºC was lower than the target value: 42.46%LHV, due to some reasons peculiar to the pilot plant: (a) two air flow meters, one installed at the inlet and the other at the outlet of the compressor, which caused pressure loss; (b) a tip clearance sensor and a pyrometer for the turbine blades which caused bypass flow of the compressed air; and (c) unexpected leak flow which directly entered the combustor from the compressor [14]. According to Figure 4, the measured power output and electrical efficiency became lower when the ambient temperature became higher, which agreed with the calculated results.

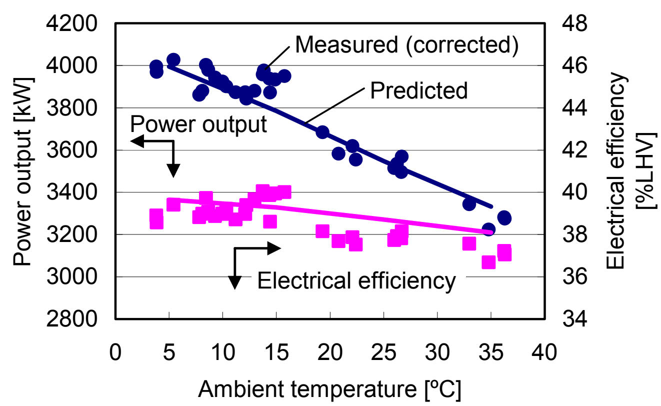

Figure 4 Measured and predicted ambient temperature effects seen in the 3MW pilot plant.

Next, the ambient temperature effects of the mid-size AHAT plant were compared with those of the CC plant using the same calculation method as the 3MW pilot plant.

Calculation of Mid-sized Plant

To calculate heat and material balance of the mid-sized AHAT and the mid-sized CC plants, the specifications of the gas turbine were assumed as given in Table 2, the same as in our past research [15]. The characteristics of the gas turbine were calculated by the in-house code which can consider stage-by-stage aerodynamics and cooling of turbine blades [5]. The size of each gas turbine was designed so that flow rate of combustion gas at the inlet of each gas turbine was the same in both plants.

Table 3 and Table 4 list the boundary conditions for the AHAT plant equipment and the CC plant equipment, respectively. The characteristics of the AHAT plant equipment, such as the WAC system and the humidification tower, were calculated as in our past studies [7,15]. However, for the CC, the HRSG (heat recovery steam generator) and the steam turbine were calculated using a commercial design program [26].

Calculation results of ambient temperature effects of the mid-sized AHAT and the CC plants are shown in Figure 5. Power output and efficiency are expressed as relative values to the respective value at base ambient temperature condition of 15ºC. Calculation results of the 3MW plant are also shown in this figure. Regarding the power output, degradation of power at high temperature was smaller for the AHAT plant because decreases of inlet air flow rate and pressure ratio at high temperature were suppressed owing to operation of the WAC. When the ambient temperature was 35ºC, power output of the AHAT plant decreased by about 5% compared to when the temperature was 15ºC, while the CC plant decreased by about 9%. In addition, degradation of power output of the 3MW pilot plant at the high temperature condition was larger than that of the CC plant even though it did not have the inlet air cooling system. This was caused by the difference of the operation characteristics of the centrifugal compressor (3MW AHAT) and the axial compressor (in the CC plant).

Table 2 Gas turbine specifications used for calculation.

Gas turbine specifications (at design point)
Type
·Single-shaft, mid-sized industrial
Inlet duct
·Ambient condition = ISO standard condition
Compressor
·Polytropic efficiency = 91.5%
·Pressure ratio = 20 : 1
Combustor
·Fuel = natural gas
·Combustion efficiency = 99.99%
Turbine
·Turbine entry temp. = 1,300ºC
·Adiabatic efficiency = 86.0%
·Coolant air flow rate = calculated
Generator
·Efficiency = 97.5%

Table 3 AHAT plant equipment specifications.

AHAT plant specifications (at design point)
WAC system
·Water flow rate = 3.5 weight % of inlet air flow
Humidification tower
·Texit,water = 110ºC
Recuperator
·Tinlet, gas – Texit, air = 40ºC
·Temperature effectiveness = 91.3%
Economizer
·Texit, gas = 110ºC
Exhaust gas reheater
·Texit, gas = 80ºC
Pressure losses
·Inlet duct = 1.1% (4.5 inch Aq.)
·Comp. exit to Comb. inlet = 6%
·Combustor = 4%
·Turbine exhaust = 5.1% (22 inch Aq.)

Table 4 CC Plant equipment specifications.

CC plant specifications (at design point)
HRSG Type
·Non-reheated, double-pressure
High pressure steam
·Steam pressure = 5MPa
·Steam temp.= Tinlet,gas – 40ºC
·ΔT_{PP}=12ºC, ΔT_{AP}=8ºC
Low pressure steam
·Steam pressure = 0.5MPa
·Steam temp.= 260ºC
·ΔT_{PP}=12ºC, ΔT_{AP}=8ºC
Pressure loss
·HRSG = 4.68% (20 inch Aq.)
Condenser
·Degree of vacuum = 5.07kPa (Tcond=33ºC)
Generator
·Efficiency = 97.5%

Regarding the electrical efficiency, the efficiency of the AHAT plant decreased slightly at high ambient temperature and so did the CC plant at low temperature. At the high temperature condition, humidity in the flue gas of the AHAT increased and it led to system heat loss. For the CC, flue gas temperature at the HRSG exit was higher at the low ambient temperature condition due to an increase of compressor inlet air flow rate while heat transfer area of the HRSG remained the same. Moreover, the assumption that the condenser vacuum remained the same value regardless of the ambient temperature condition led to the same efficiency at the high ambient temperature condition.

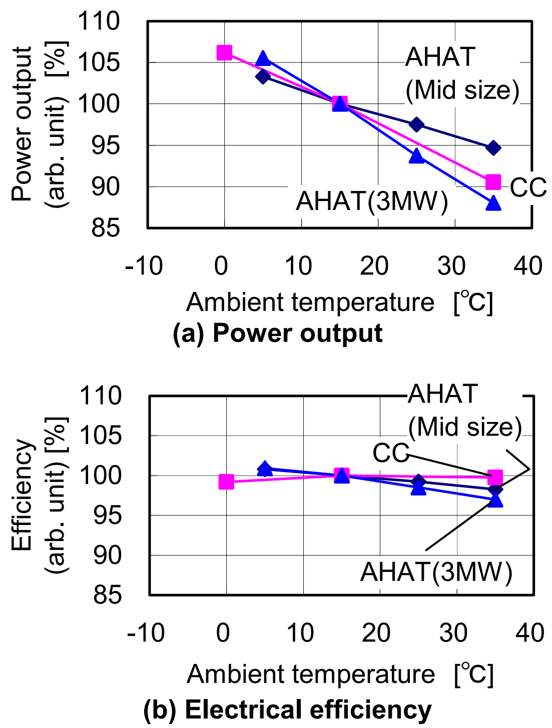

Figure 5 Predicted ambient temperature effects of the mid-sized AHAT and CC plants.

PART-LOAD CHARACTERISTICS

Part-load Characteristics of the 3MW Pilot Plant

Figure 6 shows the measured humidification rates for the humidification tower and the WAC at part-load operations of the 3MW pilot plant. From 47% -58% loads, only part of the hot water heated by the economizer and the air cooler was utilized for humidification; we call this "partial humidification." At larger loads, all the hot water was fed to the humidification tower; we call this "full humidification." The WAC was operated when the load was larger than 86%.

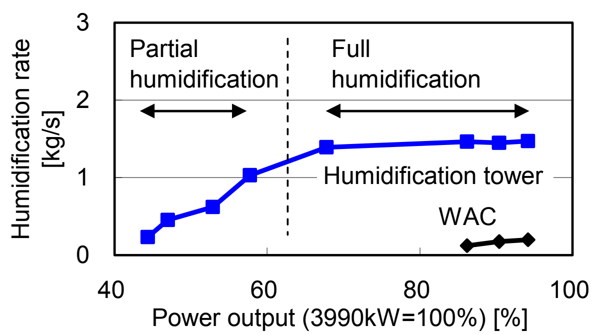

Figure 6 Measured humidification rates for the humidification tower and the WAC at part-load operations of the 3MW pilot plant.

Figure 7 compares measured and predicted electrical efficiencies at part-load operation of the 3MW pilot plant; they agreed with each other well. In the next section, the part-load characteristics of the mid-size AHAT and the CC plants were compared using the same calculation method.

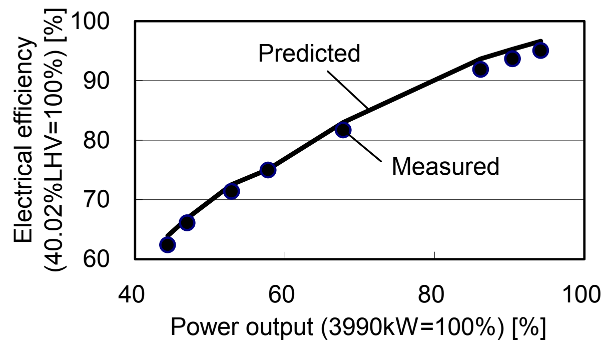

Figure 7 Measured and predicted part-load characteristics of the 3MW pilot plant.

Part-load Characteristics of the Mid-sized Plant

The gas turbine equipped with an IGV (inlet guide vane) can reduce the inlet air flow rate by closing the IGV. So, the CC plant closes its IGV, reducing the inlet air flow rate at part-load operation to keep both combustion temperature and turbine exhaust temperature high, which leads to high thermal efficiency.

To calculate part-load characteristics of the AHAT and the CC plants, the angle of the IGV and combustion temperature were assumed as in Table 5, so at the part-load operation, the power outputs of the mid-sized AHAT and the mid-sized CC plant were decreased by closing the IGV and reducing combustion temperature, while keeping their turbine exhaust temperature constant.

The lower limit of inlet air flow rate reduction by closing the IGV was assumed to be 68% of the designed air flow rate, from which we could calculate the 50% load of the AHAT. Also, the change in the compressor efficiency due to the operation of the IGV was assumed considering real gas turbine data.

Table 5 Conditions for part-load calculations.

No.	System	IGV angle	Combustion temp.
1	CC	Variable	Constant turbine exhaust temp. (566.0°C)
2	AHAT		Constant turbine exhaust temp. (603.4°C)

Figure 8 shows the calculated part-load characteristics of the AHAT and CC plants. The results of the 3MW pilot are also shown. Figure 8(a) indicates that the degradation of the electrical efficiency was smallest for the mid-sized AHAT, followed by the CC and the 3MW AHAT plants. This order of efficiency was based on the following.

Figure 8(b) shows the change in the inlet air flow rate of the compressor. The flow rates of the mid-sized AHAT and CC plants were reduced for decreasing power by closing the IGV, while the change in the flow rate of 3MW AHAT was relatively small.

Figure 8(c) shows the air temperature at the inlet of the combustor. The electrical efficiency became high if this temperature was high because less fuel was needed at the combustor. This temperature for the mid-sized AHAT plant was kept high even at part-load operation because it was the air outlet temperature from the recuperator, which was kept high owing to the constant turbine exhaust temperature operation. On the other hand, the combustor inlet air temperature for the CC plant became lower as it was the compressor outlet air temperature which became lower at part-load operation.

Figure 8(d) shows the turbine entry temperature. The turbine exhaust temperature T_4 was represented by Eq. (1) using the turbine entry temperature T_3. As shown by Table 6, the specific heat ratio γ was smaller for humid air. According to this equation, when the turbine exhaust temperature T_4 was kept constant and the pressure ratio p_3/p_4 became smaller at part-load operation, the turbine entry temperature T_3 of the AHAT plant became higher than that of the CC plant.

$$\frac{T_4}{T_3} = \left(\frac{p_4}{p_3}\right)^{\eta_p \frac{\gamma-1}{\gamma}} \qquad (1)$$

Table 6 Specific heat ratios of air and water.

Items	Air	H_2O	Remarks
Cp: Constant pressure specific heat [kJ/kgK]	1.143	2.300	at 1000K, 1MPa
γ: Specific heat ratio [-]	1.337	1.257	$\gamma = C_P/C_V$
$(\gamma-1)/\gamma$ [-]	0.252	0.204	

Figure 8(e) shows the turbine exhaust temperature change. The turbine exhaust temperature (Table 5) was set to a constant value for the mid-sized AHAT and CC plants. On the other hand, the turbine exhaust temperature of the 3MW AHAT became lower with decreasing power output because it did not have the IGV.

Finally, as shown by Figure 8(c) and Figure 8(d), because the air temperature at the combustor inlet and at the turbine inlet could be kept higher, the electrical efficiency of the AHAT system could be kept higher at part-load operation.

START-UP CHARACTERISTICS

Turbine speed, power output, humidification rate, and turbine entry temperature of the 3MW AHAT pilot plant during the cold start-up are shown in Figure 9. After purging the duct at about 20% turbine speed (Figure 9(a)), the combustor was ignited 9min after the start command and the turbine speed was

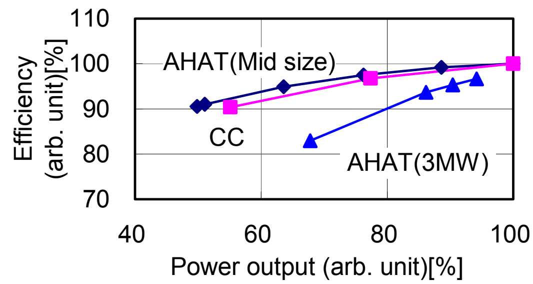

(a) Electrical efficiency

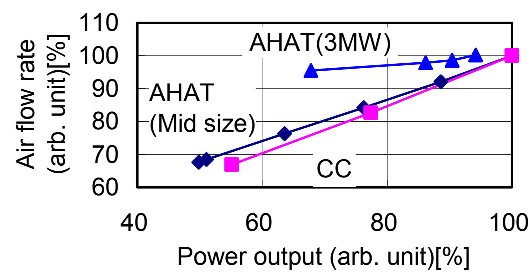

(b) Compressor inlet air flow rate

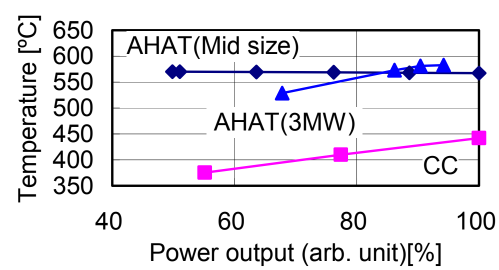

(c) Combustor inlet air temp.

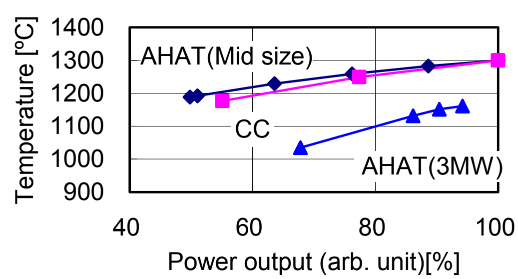

(d) Turbine entry temp.

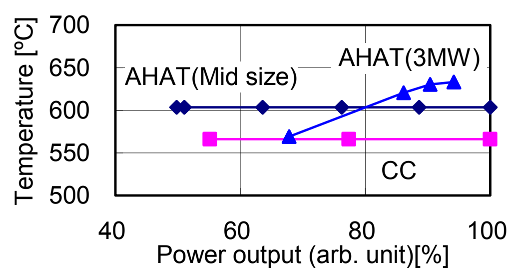

(e) Turbine exhaust gas temp.

Figure 8 Part-load characteristics of AHAT and CC plants.

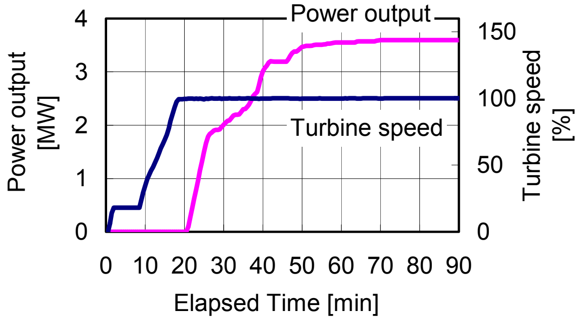

(a) Turbine speed and power output

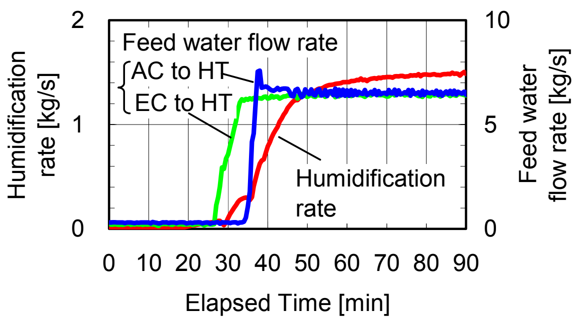

(b) Humidification

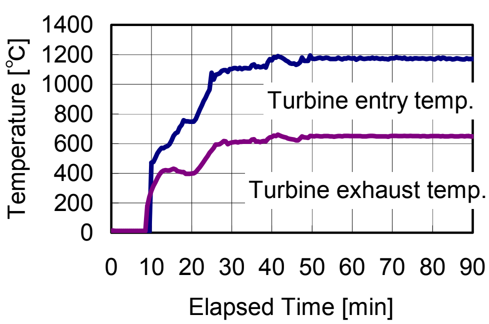

(c) Turbine entry temperature

Figure 9 Turbine speed, power output, humidification rate, and turbine entry temperature of the 3MW AHAT pilot plant during the start-up.

increased to full speed 20min after the start command. The power output was increased at a rate of 10%/min and the power reached 1800kW; this was about 50% load 26min after the start command. Then, hot water generated by the EC (economizer) and AC (air cooler) was consecutively fed to the HT (humidification tower), which increased the humidification rate (Figure 9(b)).

Then, the turbine exhaust temperature reached 650ºC 41min after the start command (Figure 9(c)), and the power was held at 3200kW until 46min after the start command. This was followed with warming up of heat recovery equipment such as the recuperator or the economizer, and humidification rate was increased (Figure 9(b)). Finally, 60min after the start command, the power output was increased to 3550kW keeping the turbine exhaust temperature under 650ºC.

This start-up method is similar to that of the first start-up method of the EvGT pilot plant [20] which integrated the gas turbine and the water circuit at about 15% load. One of the reasons why the cold start-up time of the 3MW AHAT (60min) was longer than that of the EvGT (45min) is the heat capacity of the recuperator. The former uses the rigid-type, plate-fin recuperator while the latter used the lightweight, primary surface type recuperator. Moreover, the AHAT is equipped with an exhaust gas reheater to prevent plume formation, which enlarges the heat capacity of the water circuit. Additionally, the start-up sequence of the AHAT pilot plant includes purging of the exhaust gas duct for about 7min for safety.

As a result of this start-up test, we recognized that the humidification rate at the humidification tower needed to reach the maximum value to get the maximum power output, which required a warming of the economizer. Warming of the economizer required warming of the recuperator located upstream from the economizer. Therefore, the start-up time of the AHAT was mainly dominated by the heat capacity of the recuperator.

In the present study, we did not test the second start-up method at the EvGT pilot plant, by which the gas turbine was started with the humidification process fully integrated from the beginning. One of the reasons why we did not was to avoid an inflow of humid air into the recuperator and the gas turbine before they are warmed, which causes a large amount of condensation inside them.

CHARACTERISTICS OF THE RECUPERATOR

Specifications of the Recuperator

For a recuperator of the 3MW AHAT pilot plant, a plate-fin type heat exchanger, which has the merit of high temperature effectiveness and compactness, has been developed. Table 7 lists the designed specifications of the

Table 7 Designed specifications of the recuperator.

Items		Exhaust gas side	Air side
Flow rate [kg/s]		11.9	10.4
Abs. humudity [kg/kg']		0.20	0.18
Inlet temp. [ºC]		668.1	116.4
Outlet temp. [ºC]		231.9	629.6
Temp. effectiveness [%]		-	93.0
Operating pres. [kPaG]		7.4	699.9
Pres. loss [%]		4.1	1.8
No. of blocks [-]		4	
Size of each block [mm]		W 600 x H 1157 x L 850	
Type of fin [-]		Perforated fin	Offset fin
Material	Fin	NAR-AH-7	
	Tube plate	NAR-AH-7 (3 blocks) HASTELLOY(R) X (1 block)	
	Side plate		
	Spacer bar	SUS310S	

recuperator. The recuperator consisted of four blocks, which were connected to the humid air piping and the exhaust gas duct in parallel. Figure 10 and Figure 11 are photos of the heat exchanger block and the whole assembly installed in the 3MW pilot plant, respectively. A perforated fin was used for the exhaust gas side considering not only heat transfer but also pressure loss, while an offset fin, which had a higher heat transfer coefficient, was used for the air side. A heat-resistant, oxidation-resistant austenitic stainless steel, NAR-AH-7 [27], which contains optimal amounts of chrome, nickel and rare-earth elements, was used for the corrugated fin, tube plate and the side plate. This material resists high-temperature, high-humidity combustion exhaust gas, even when used in the form of thin sheets.

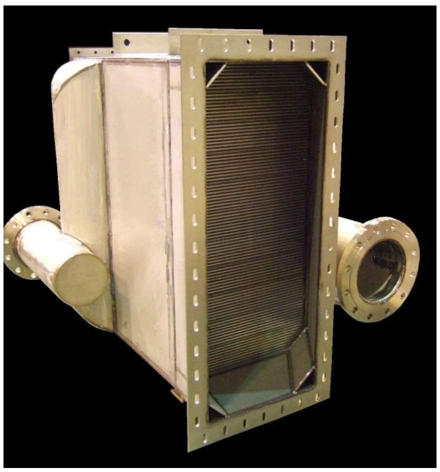

Figure 10 Photo of the heat exchanger block.

Figure 11 Photo of the installed recuperator.

Pressure Drops and Temperature Effectiveness

Humid air of the AHAT contains about 20 vol% water vapor unlike in an ordinary gas turbine. To confirm whether or not unexpected problems such as corrosion of the material or blockage of the flow channel occur, interannual changes in pressure drops, temperature effectiveness, and overall heat transfer coefficient of the recuperator were evaluated.

Figure 12 shows interannual changes of the gas side and air side pressure drops of the recuperator from February 2007 to February 2010 when the humidification tower was operated. There were 17 runs in total and their cumulative time was about 80 hours.

Because the flow rates and the pressure of the fluid fed to the recuperator differed day to day depending on the ambient conditions, the measured values were corrected as follows. The pressure drops at the exhaust gas side and at the air side of the whole recuperator assembly were corrected by the following equations, respectively.

$$\frac{\Delta P_{g,0}}{\Delta P_g} = \frac{\rho_g}{\rho_{g,0}} \cdot \left(\frac{G_{g,0}}{G_g} \right)^{1.29} \quad (2)$$

$$\frac{\Delta P_{a,0}}{\Delta P_a} = \frac{\rho_a}{\rho_{a,0}} \cdot \left(\frac{G_{a,0}}{G_a} \right)^{1.7} \quad (3)$$

The exponent 1.29 in Eq. (2) was derived from correlations of friction factor for the offset strip fin presented by Wieting [28]. On the other hand, for the air side, the exponent 1.7 in Eq. (3) was derived by averaging the friction factors for the offset strip fin and other pressure drop elements of the piping such as elbows, bends and tees.

According to Figure 12, there was no significant change in the air side pressure drop, and deviation was relatively small during this period. The gas side pressure drop did not increase during this period, but the deviation was larger than that of the air side. This must be caused by the change of the spray water flow rate of the water recovery system. The flow rate of the spray nozzle affected the pressure distribution inside the exhaust gas duct, which was varied according to the test conditions of the water recovery system.

On the other hand, change of the overall heat transfer coefficient was corrected assuming the following simplifications: (a) each heat transfer coefficient of the air side and the gas side was proportional to the 0.46th power of each mass flow rate; (b) thermal resistance of the air side and the gas side were equal at the standard condition; (c) thermal resistance of the tube plate between the air flow and the gas flow was zero. From these assumptions, the overall heat transfer coefficient K at a certain operation condition was represented as follows:

$$\frac{K_0}{K} = \frac{1}{2}\left[\left({G_{a,0}}/{G_a} \right)^{0.46} + \left({G_{g,0}}/{G_g} \right)^{0.46} \right] \quad (4)$$

The exponent 0.46 was also derived from correlations of Colburn j-factor for the offset strip fin [28].

Interannual changes of the overall heat transfer coefficient corrected by the above assumption and the temperature effectiveness of the air side calculated by Eq. (5) are shown in Figure 13. There was no significant change in the overall heat transfer coefficient and the temperature effectiveness of the recuperator. The temperature effectiveness was around 93% during this period.

$$\varepsilon_a = \frac{T_{a,o} - T_{a,i}}{T_{g,i} - T_{a,i}} \quad (5)$$

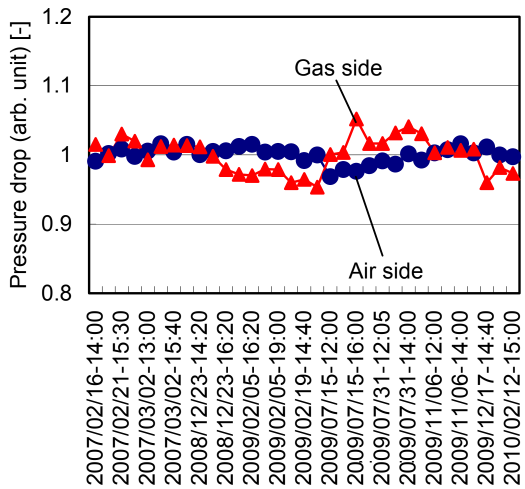

Figure 12 Interannual changes of gas side and air side pressure drops of the recuperator.

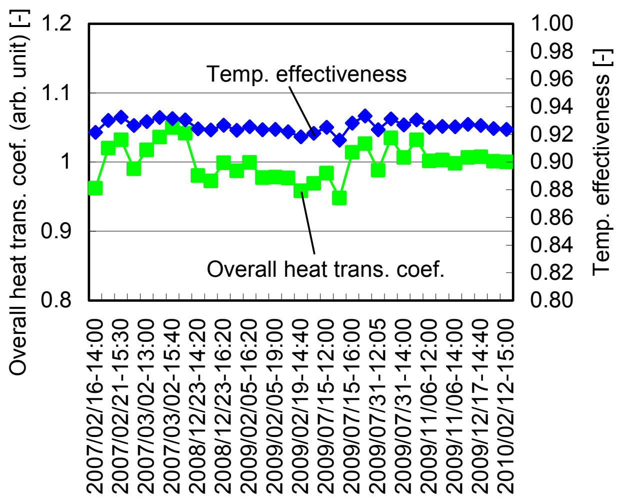

Figure 13 Interannual changes of the overall heat transfer coefficient and the temperature effectiveness of the recuperator.

CONCLUSIONS

Ambient temperature effects, part-load characteristics, and start-up characteristics of the 3MW AHAT pilot plant were measured along with a change in heat transfer characteristics of the recuperator. By using the same calculation method as for the 3MW pilot plant, ambient temperature effects and part-load characteristics of the mid-sized AHAT plant were compared with the CC plant. The results are summarized as follows.

(1) Ambient temperature effects

The power output and electrical efficiency of the 3MW pilot plant became lower with high ambient temperature, which agreed with the calculation results.

Degradation of power output at the high temperature condition was smaller for the mid-sized AHAT plant owing to the WAC. When the ambient temperature was 35ºC, power output of the mid-sized AHAT decreased by about 5% compared to when the temperature was 15ºC, while the CC decreased by about 9%.

The electrical efficiency of the AHAT decreased slightly at high ambient temperature and so did the CC at low temperature. The assumption that the condenser vacuum value remained the same regardless of the ambient temperature condition led to the same efficiency of the CC at the high ambient temperature condition.

(2) Part-load characteristics

The measured and predicted electrical efficiencies of the 3MW pilot plant at part-load operation agreed with each other. The degradation of the electrical efficiency for the mid-sized AHAT plant was smaller than for the CC plant. The respective efficiencies decreased by 6.2% and 8.0%, at 60% load operation.

(3) Start-up characteristics

The start-up time of the AHAT was mainly dominated by the heat capacity of the recuperator. The cold start-up time of the 3MW AHAT pilot plant was 60min after the start command.

(4) Characteristics of the recuperator

Interannual changes from February 2007 to February 2010 for pressure drops, temperature effectiveness, and overall heat transfer coefficient of the recuperator were evaluated. There were no degradations in these characteristics. The temperature effectiveness was around 93% during this period.

ACKNOWLEDGMENT

This research was made possible by the assistance of the Ministry of Economy, Trade and Industry of Japan, Agency for Natural Resources and Energy. We wish to express our deep gratitude for this support.

NOMENCLATURE

C_p	Constant pressure specific heat [kJ/kgK]
E	Electrical efficiency [%LHV]
f	Correction factor [-]
G	Mass flow rate [kg/s]
K	Overall heat transfer coefficient [W/m^{2}K]
T	Temperature [ºC]

T_3 Turbine entry temperature [ºC]
T_4 Turbine exit temperature [ºC]
P Power output [kW]
p_3 Turbine entry pressure [kPa]
p_4 Turbine exit pressure [kPa]
u Velocity [m/s]

Subscripts

0 Standard conditions
a Air side
i Inlet
g Exhaust gas side
o Outlet

Greek symbols

α Overall correction factor for power output [-]
β Overall correction factor for electrical efficiency [-]
ΔP Pressure drop [Pa]
ΔT_{AP} Approach point temperature difference [K]
ΔT_{PP} Pinch point temperature difference [K]
ε Temperature effectiveness [-]
η_p Polytropic efficiency [-]
ρ Density [kg/m^3]

REFERENCES

1. The House of Councilors, National Diet of Japan, "Basic Act on Global Warming Countermeasures," http://www.sangiin.go.jp/japanese/joho1/kousei/gian/174/meisai/m17403174052.htm [in Japanese]
2. The Ministry of Economy, Trade and Industry of Japan, "Basic Policy for Energy Demand and Supply," http://www.meti.go.jp/committee/summary/0004657/energy.pdf [in Japanese]
3. Hatamiya, S., 2002, "Gas Turbine Power Generation Technology Utilizing High Humidity Air," The Thermal and Nuclear Power, **53**(9), pp. 1031-1038. [in Japanese]
4. Takahashi, T., Koda, E. and Mimaki, T., 2002, "A Systematic Analysis of the Effect of Air Humidification to Gas Turbine Systems," JSME International Journal Series B, **45**(3), pp. 530-535.
5. Higuchi, S., Hatamiya, S., Seiki, N. and Marushima, S., 2003, "A Study of Performance on Advanced Humid Air Turbine Systems," *IGTC 2003*, Tokyo, TS-090.
6. Hatamiya, S., Araki, H. and Higuchi, S., 2004, "An Evaluation of Advanced Humid Air Turbine System with Water Recovery," ASME GT2004-54031.
7. Araki, H., Higuchi, S., Marushima, S. and Hatamiya, S., 2005, "Design Study of a Humidification Tower for the Advanced Humid Air Turbine System," ASME 2005-GT-68671.
8. Kuroki, H., Shibata, T., Koganezawa, T., Kizuka, N., Hatamiya, S. and Marushima, S., 2006, "Development of Elemental Technologies for Advanced Humid Air Turbine System," ASME GT2006-90639.
9. Koganezawa, T., Miura, K., Saito, T., Abe, K. and Inoue, H., 2007, "Full Scale Testing of a Cluster Nozzle Burner for the Advanced Humid Air Turbine," ASME GT2007-27737.
10. Takahashi, T., Nakao, Y. and Koda, E., 2007, "Analysis and Evaluation about Advanced Humid Air Turbine System," *ICOPE 2007*, Hangzhou, China, E060
11. Araki, H., Katagiri, Y., Marushima, S., Hatamiya, S., Higuchi, S. and Tsukamoto, M., 2007, "Experimental Results of Humidification and Water Recovery of the Advanced Humid Air Turbine System Pilot Plant," *IGTC 2007*, Tokyo, TS-012.
12. Katagiri, Y., Araki, H., Koganezawa, T., Hatamiya, S., Marushima, S., "Humidity and Plant Control System for the Advanced Humidified Air Turbine Pilot Plant," *IGTC 2007*, Tokyo, TS-013.
13. Higuchi, S., Koganezawa, T., Horiuchi, Y., Araki, H., Shibata, T. and Marushima, S., 2008, "Test Results from the Advanced Humid Air Turbine System Pilot Plant – Part 1: Overall Performance," ASME GT2008-51072.
14. Araki, H., Higuchi, S., Koganezawa, T., Marushima, S., Hatamiya, S. and Tsukamoto, M., 2008, "Test Results from the Advanced Humid Air Turbine System Pilot Plant – Part 2: Humidification, Water Recovery and Water Quality," ASME GT2008-51089.
15. Araki, H., Koganezawa, T., Myouren, C., Higuchi, S., Takahashi, T. and Eta, T., 2010, "Operation Characteristics of the AHAT system," *Proceedings of the 38th GTSJ Annual Meeting*, Tokushima, Japan, C4. [in Japanese]
16. Nakamura, H. and Yamamoto, K., 1992, "HAT (Humid Air Turbine) Cycle," The Thermal and Nuclear Power, **43**(12), pp. 1587-1592. [in Japanese]
17. Mori, Y., Nakamura, H., Takahashi, T. and Yamamoto, K., 1983, "A Highly Efficient Regenerative Gas Turbine System by New Method of Heat Recovery with Water Injection," *IGTC 1983*, Tokyo, pp. 297-303.
18. Rao, A. D., Francuz, V. J., Shen, J. C. and West, E. W., 1991, "A Comparison of Humid Air Turbine (HAT) Cycle and Combined-Cycle Power Plants," EPRI IE-7300 Project 2999-7 Final Report.
19. Lindquist, T. O., Rosén, P. and Torisson, T., 2000, "Theoretical and experimental evaluation of the EvGT-process," ASME AES, **40**, pp. 457–469
20. Lindquist, T. O., Rosén, P. and Torisson, T., 2000, "Evaporative Gas Turbine Cycle – A Description of a Pilot Plant and Operating Experience," ASME AES, **40**, pp. 511-520.
21. Lindquist, T. O., Thern, M. and Torisson, T., 2002, "Experimental and Theoretical Results of a Humidification Tower in an Evaporative Gas Turbine Cycle Pilot Plant," ASME GT-2002-30127.
22. Ågren, N. D., Westermark, M. O., Bartlett, M. A. and Lindquist, T. O., 2000, "First Experiments on an Evaporative Gas Turbine Pilot Power Plant: Water Circuit Chemistry and Humidification Evaluation," ASME 2000-GT-0168.

23. Lorenz, M., 2004, "Modeling and Off Design Simulation of the Evaporative Gas Turbine," Studienarbeit, Department of Heat and Power Engineering, Lund Institute of Technology, Lund University, Lund, Sweden.
24. Wang, B., Zhang, S. and Xiao, Y., 2007, "Steady-State Off-Design Performance of Humid Air Turbine Cycle," ASME GT2007-27350.
25. Akiyoshi, R., Imai, K., Sioda, T., Ito, K. and Hori, M., 2003, "Development of Large Scale Recuperator for Gas Turbine," *IGTC 2003*, Tokyo, TS-112.
26. Thermoflow, Inc., "GT PRO," http://www.thermoflow.com/CombinedCycle_GTP.htm.
27. Nishiyama, Y., Otsuka, N., Kitamura, K. and Abe, M., 2010, "Development of Heat Resistant Stainless Steel Sheet <NAR-AH-7> for Advanced High-Temperature Recuperators," Materia Japan, **49**(2), pp. 72-74. [in Japanese]
28. Wieting, A., R., 1975, "Empirical Correlations for Heat Transfer and Flow Friction Characteristics of Rectangular Offset-Fin Plate-Fin Heat Exchangers," ASME, Journal of Heat Transfer, **97**(3), pp. 488-490.

APPENDIX

To evaluate the ambient temperature effects of the 3MW AHAT plant, power output and electrical efficiency measured under various operational conditions were corrected as if they were operated at the base conditions listed in Table 8.

Table 8 Base conditions assumed to correct the measured power output and electrical efficiency.

Item	Unit	Value
Turbine entry temperature	ºC	1,180
WAC flow ratio (inlet air flow basis)	%	1.5
Ambient pressure	kPa	101.3
Relative humidity	%	60
Combustion efficiency	%	99.99
Recirculation water flow rate to EGR	kg/s	0

Correction of power output

Corrected power output P_c was calculated from measured power output P_m and an overall correction factor α by Eq. (6). The overall correction factor α was expressed by Eq. (7) using correction factors $f_{P,j}$ which represent the change of power output due to the change of turbine entry temperature (j=1), WAC flow ratio (j=2), ambient pressure (j=3), relative humidity (j=4), combustion efficiency (j=5) and recirculation water flow rate to EGR (j=6). These factors were represented as a polynomial function of each operational condition, which was derived from the heat and material balance calculation.

$$P_c = P_m \times \frac{1}{\alpha} \quad (6)$$

$$\alpha = \prod_{j=1}^{6} \left(1 + \frac{f_{P,j}}{100} \right) \quad (7)$$

Correction of electrical efficiency

Similarly, corrected electrical efficiency E_c was calculated from measured electrical efficiency E_m and an overall correction factor β by Eq. (8). The overall correction factor β was expressed by Eq. (9) using correction factors $f_{E,j}$ which represent the change of electrical efficiency. These factors were derived in the same way as the correction of power output.

$$E_c = E_m \times \frac{1}{\beta} \quad (8)$$

$$\beta = \prod_{j=1}^{6} \left(1 + \frac{f_{E,j}}{100} \right) \quad (9)$$